Energy and Accuracy Characterization of a Burst-Mode Range Sensing Approach for Smart Contact Lenses

Sakthidasan Kalidasan, Chayanjit Ghosh, Adwait P. Deshpande, Carlos H. Mastrangelo and Ross Walker
ECE Department, University of Utah, Salt Lake City, USA
sakthidassakthidas97@gmail.com

***Abstract*— In this paper, we present the characterization of a new range sensing approach for use in emerging smart contact lens applications. Smart contact lenses offer a promising approach to treating the most common form of vision loss by using a tunable lens to accommodate for focal errors. A range sensor is an integral component of the system because it estimates an object's distance from the user in order to determine the target focal length. We performed an empirical study with custom fabricated coils in a mock eyeball setup to understand the energy-accuracy trade-offs of a burst-mode sensing approach based on transmission and reception of square pulses between the coils. We wirelessly transmitted square pulses between the coils and estimated the range of an object by sensing the received voltages and inferring the angular relationship between the two contacts. We demonstrate a functioning range sensing approach that can be implemented with energy as low as 1.8 nJ per measurement with at least 95% accuracy.**

I. Introduction

Presbyopia is a gradual loss of focal accommodation of the eye with age, resulting in loss of image focus, blurry vision, and other visual impairments. It has been estimated that about 108 million people are suffering from presbyopia in North America alone, and 1.04 billion globally [1]. Smart contact lenses offer a promising approach for correcting focal errors without the need for eyeglasses with complicated lens designs [2]-[8]. Smart contact lenses can use electrically tunable lenses to continuously adapt to the object of interest within the user's focal range. In order for such a system to work, a range sensor is needed to determine the distance of the object from the user's eyes. The range sensor estimates the distance to the object of interest and passes the information to a micro-controller, which determines whether the focal length of the lens needs to be adjusted. Then an appropriate control voltage will be applied to the tunable lens, which will correct the focal length. The smart contact lens system concept is illustrated in Figure 1.

In [2] we presented a preliminary prototype for a range sensing approach using weakly coupled coils. We demonstrated that by exploiting the angular dependence of the coupling coefficient between two coils, the range of an object could be estimated. Since the coupling coefficient directly affects the voltage transfer across the coils, it is possible to arrive at an estimate of the range of the object by transmitting a signal through one coil and measuring the received voltage on the other coil. Proof of concept was shown using bench-top measurements without any custom electronics. While this

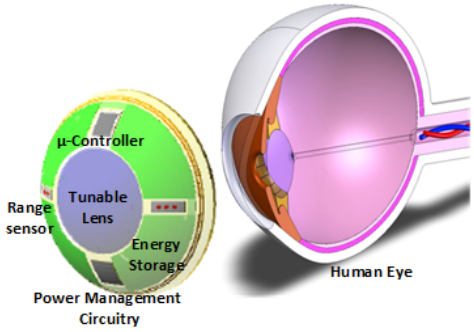

Fig. 1: Smart contact lens concept for vision correction

was useful in establishing proof of concept for this range sensing approach, it was far from a practical implementation. Any practical approach needs to be highly energy efficient for integration into smart contact lenses, which are standalone wireless systems where energy is a scarce resource. In this paper, we present characterization of a burst-mode range sensing approach to explore opportunities for achieving energy efficiency without much loss of accuracy.

We used an empirical process to determine appropriate design parameters, since accurate modelling and closed-form analysis is confounded by the physics of the system. The bench-top system used for characterization is used here as a tool to show a clear dependence of accuracy on energy consumption, in order to understand the practical limitations of this burst-mode range sensing approach.

Section II discusses the burst-mode operation used to improve energy efficiency and including theory and the performance parameters we used to characterize the approach. Section III presents measurements and results. Section IV concludes the paper with a summary of the work and future directions.

II. Burst-Mode Range Sensing Approach

Figure 2 shows an illustration of the range sensing approach using inner and outer coils integrated into each contact lens. We apply an input signal with an amplitude of V_{Tx} into the transmitter. N_{cycles} denotes the number of cycles sent through the transmitter during burst mode. If only one coil configuration is used to extract the θ_L and θ_R angles, there is a possibility of having the same received voltage

2022 IEEE Sensors | 978-1-6654-8464-0/22/$31.00 ©2022 IEEE | DOI: 10.1109/SENSORS52175.2022.9967207

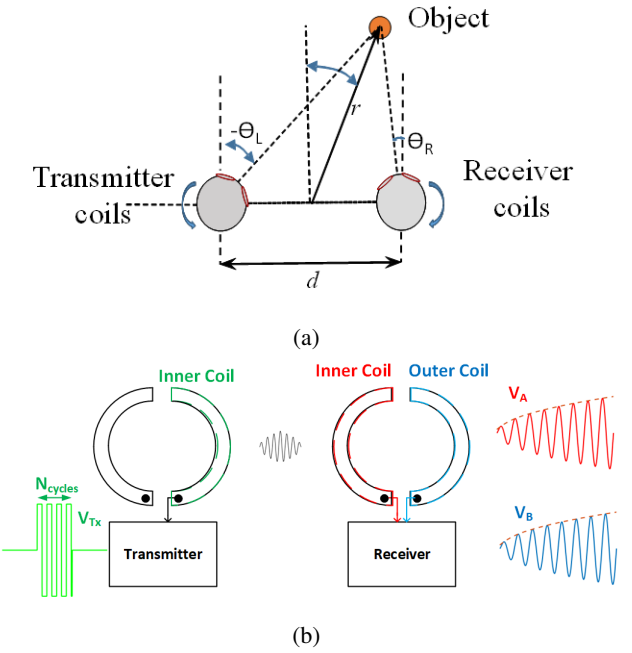

Fig. 2: (a) Schematic of object distance ranging via triangulation of eyeball angles, (b) Transmit and receive coil configurations for extracting the received V_A and V_B voltages, V_A and V_B are the received voltages for the inner-inner and inner-outer configurations respectively.

for different pairs of θ_L and θ_R. Hence we use the Inner-Inner and Inner-Outer configurations shown in Figure 2b to generate the a pair of received voltages, V_A and V_B, which have even and odd functional characteristics respectively. The combination of an even (V_A) and odd (V_B) function makes it possible to generate an inverse function to extract θ_L and θ_R. From the set of angles, the object distance r can be derived as:

$$r = \frac{d * cos(\theta_L)cos(\theta_R)}{sin(\theta_L - \theta_R)cos((\theta_L + \theta_R)/2)} \quad (1)$$

where d is the distance between the eyes.

We generate a pair of calibration plots that are used to determine the range based on the received voltages. The calibration plots are constructed by averaging the received voltages over many transmits cycles to reduce random variations. By storing the calibration plots as a lookup table, range estimation is simplified compared to an analytical model of the received voltage response, which would require complicated equations even in idealized or approximate models. The sensing approach relies on wirelessly transmitting some type of signal between the coils. We choose square pulses because 1) they generate a larger voltage response at the receiver than other waveforms and 2) they are straightforward and energy efficient to produce using digital electronics. One way to reduce energy is by reducing the number of cycles (N_{cycles}) sent by the transmitter. This reduces the overall energy consumption by reducing the total energy delivered into the transmitter coil and also by reducing the time the receiver needs to be on. Hence, N_{cycles} can be used as a parameter to effectively optimize the overall accuracy and energy requirements of the range sensor. In order to extract a low-noise indicator of the coupling coefficient, we use the envelope of the received signal as the measurement metric instead of the peak to peak voltage [9]. The inherent averaging in the envelope helps to reduce the impact of the high-frequency noise and hence improves the SNR of the measurement.

III. Measurements and Results

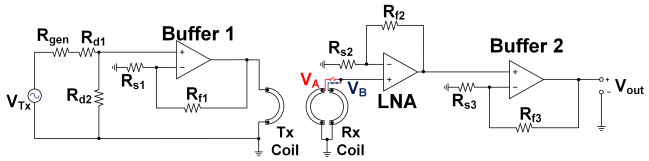

Fig. 3: Custom PCB circuit used to characterize the range sensing approach

The range sensor demonstration in [2] was limited because a) the signal generator's series resistance hindered the maximum power that can be transferred to the coil, and also (b) the achievable resonance frequency was reduced by the coaxial cables parasitic capacitance, which in return reduced the maximum gain that can be achieved across the coils. In order to deal with these issues, we designed the circuit shown in Figure 3 using commercially available components to demonstrate a functioning range sensor with more practical signal levels and frequency.

ADA4807 was used for implementing buffers in the bench-top design, and the low noise amplifier was implemented using LTC6268. Custom coils were designed, fabricated, and mounted on motorized mock eyeballs as shown in Figure 4. Using a buffer to drive the transmit coil solves the maximum power transfer issue and also increases the coil system's resonance frequency by decoupling the transmit coil from the coaxial cable used for testing. Adding a receiver amplifier improves the overall gain, which helps reduce the voltage amplitude that needs to be driven into the transmit coil, thus enabling power savings.

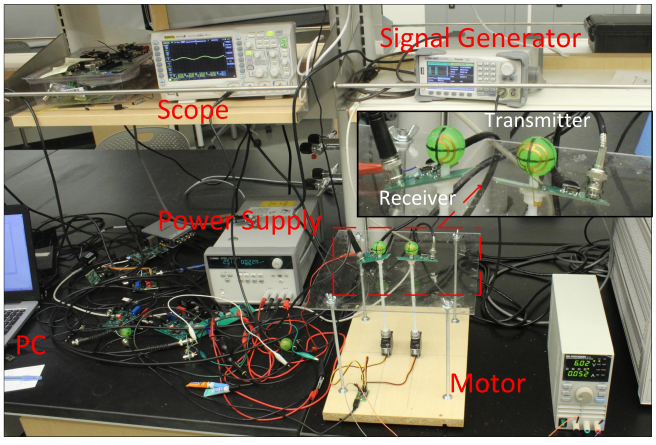

Fig. 4: Laboratory test setup used for characterization

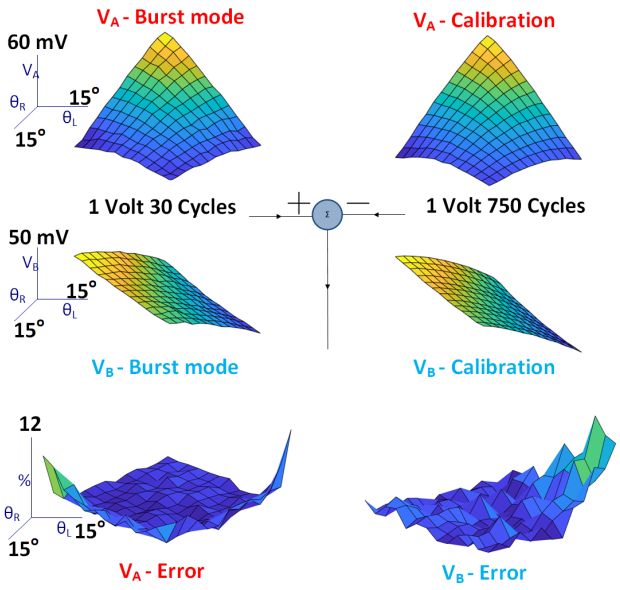

Fig. 5: System measurements and results - Top left: V_A Burst mode plot; Top right: V_B calibration plot; Mid left: V_B Burst mode plot; Mid right: V_B calibration plot; Bottom left: V_A error plot; Bottom right: V_B error plot;

The resonance frequency of the coils was measured to be 19.8 MHz, which is chosen as the operating frequency for the system. A supply voltage of 5 V was used to power the electronics. The measured gain of the receiver amplifier was 20 V/V and the total measured power of the receiver electronics was 120 mW for the bench-top characterization system. This power level is far higher than needed, e.g. in a custom ASIC implementation, where bias current can be minimized to tightly meet a noise specification.

The laboratory test setup used for characterization is shown in Figure 4. A PC was used to control the setup and to record the oscilloscope measurements. A motor was used to change θ_L and θ_R appropriately for measuring the received voltages at various angle combinations. θ_L and θ_R values were swept between the range of $-15°$ to $+15°$ with an angle spacing of $2.5°$. A faraday cage was used during the measurements to minimize the impact of ambient noise on the system. Post-processing was done in MATLAB for envelope extraction before generating the 3D plots for V_A and V_B shown in Figure 5.

When operating in burst mode with a low number of transmitted cycles, the noisy response plots were normalized to and then subtracted from the calibration plots to produce the error surfaces shown in Figure 5, which are used to quantify the accuracy. The mean absolute error when using 1 Vpp and 30 cycles of burst mode operation was 1.8%, the maximum error was 10.7% and the mean squared error across the error surfaces was 2.7%. Estimated range as a function of V_A and V_B for burst mode operation is shown in Figure 6, based on extraction of θ_L and θ_R from the calibration plots and estimation of range based on (1).

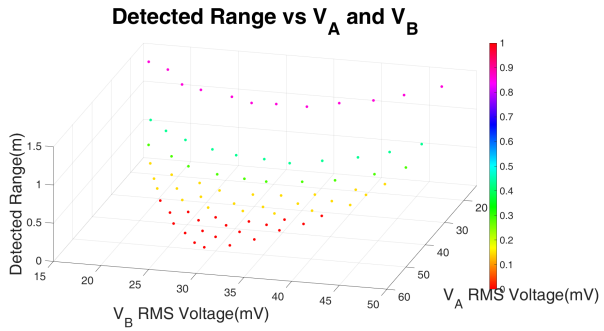

Fig. 6: Estimated range as a function of V_A and V_B in burst mode operation with 1V input and 30 cycles

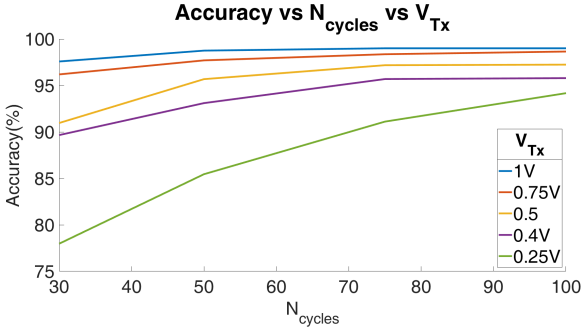

Fig. 7: Accuracy of the burst mode plots as a function of V_{Tx} and N_{cycles}. Accuracy is estimated using the mean absolute error (MAE) of the burst mode plots. Accuracy = (1-MAE)*100

Refractive power is expressed in Diopter (D) which is the inverse of the focal length. From Figure 6 the corresponding refractive power values can be estimated. The range sensing approach demonstrated here has a tuning range between 0.5D and 8D.

Accuracy vs V_{Tx} and N_{cycles} is shown in Figure 7. Accuracy estimations for a set of transmit amplitudes in the range of 0.25 V to 1 V and N_{cycles} values in the range of 30 to 100 were used to generate the plot. The plot shows that accuracy depends on both V_{Tx} and N_{cycles}, and it can be observed that better accuracy is achieved with higher V_{Tx} and N_{cycles}, at the cost of reduced energy efficiency.

IV. Conclusion

We have presented the characterization of a burst-mode range sensing approach for smart contact lenses. We demonstrated the dependence of accuracy on the transmit amplitude and number of cycles using a bench-top laboratory system that consumes about 180 nJ per measurement. We estimate that this energy consumption can be reduced by two orders of magnitude to 1.8 nJ when implemented with a custom ASIC.

Acknowledgment

This work has been supported by the National Science Foundation grant CNS-1932602.

REFERENCES

[1] B. A. Holden et al., "Global vision impairment due to uncorrected presbyopia.," Arch Ophthalmol, vol. 126, no. 12, pp. 1731–1739, Dec. 2008, doi: 10.1001/archopht.126.12.1731.

[2] C. Ghosh et al., "Low-Profile Induced-Voltage Distance Ranger for Smart Contact Lenses," IEEE Trans Biomed Eng, vol. 68, no. 7, pp. 2203–2210, Jul. 2021, doi: 10.1109/TBME.2020.3040161.

[3] C. Ghosh et al., "A Nano-Joule Burst-Mode Eye-Gaze Angle and Object Distance Sensor for Smart Contact Lenses," in 2021 IEEE Sensors2021,pp.1–4,doi:10.1109/SENSORS47087.2021.9639572.0.

[4] A. Banerjee et al., "Low-power, thin and flexible, stacked digital LC lens for adaptive contact lens system with enhanced tunability," 2021 Conference on Lasers and Electro-Optics, CLEO 2021 - Proceedings, pp. 8–9, 2021, doi: 10.1364/cleo_at.2021.af2q.8.

[5] J. Park et al., "Soft, smart contact lenses with integrations of wireless circuits, glucose sensors, and displays," Sci Adv, vol. 4, no. 1, p. eaap9841, 2018, doi: 10.1126/sciadv.aap9841.

[6] J. Park et al., "Printing of wirelessly rechargeable solid-state supercapacitors for soft, smart contact lenses with continuous operations," Sci Adv, vol. 5, no. 12, p. eaay0764, 2019, doi: 10.1126/sciadv.aay0764.

[7] J. Kim et al., "A soft and transparent contact lens for the wireless quantitative monitoring of intraocular pressure," Nat Biomed Eng, vol. 5, no. 7, pp. 772–782, 2021, doi: 10.1038/s41551-021-00719-8.9.

[8] J. Bailey et al., "Switchable liquid crystal contact lenses for the correction of presbyopia," Crystals (Basel), vol. 8, no. 1, 2018, doi: 10.3390/cryst8010029.